Fast wettability assessment on small rock samples using a 3D, high-resolution, image-based Amott-like test

Maria Repina*, *Regis* Brugidou, *Alexandre* Dufour and *Richard* Rivenq

TotalEnergies OneTech, CSTJF 64000 Pau, France

Abstract. In this paper, we propose a new experimental set-up to carry out a full Amott-like cycle on small core samples (4 mm. diameter, 15 mm. length), imaged with a high-resolution micro-CT scanner. We conduct this experiment on two core samples from a carbonate reservoir. Each step of the cycle was followed by a 3D high-resolution scan along the entire sample length and analysed using digital image-processing algorithms. The characterization of wettability is based on multiple criteria: a) a pseudo-wettability index, analogous to the Amott-Harvey index, calculated from both resolved and unresolved pores; b) experimental observations during the spontaneous phases, and c) analysis of the spatial fluid distribution in the pore space. This new type of experiment has several advantages: a) it respects the experimental sequence of the industry standard Amott test, yet with a significantly reduced test duration; b) it provides complementary information describing the spatial distribution of the fluids in the visible pore network during spontaneous and forced phases; c) it is less sensitive to imaging resolution than existing approaches based on topological characteristics and contact angles.

1 Introduction

Wettability is a key factor controlling multi-phase flow in porous media. The standard and well-established laboratory procedures used to characterize the wettability of an oil/brine/rock system in the O&G industry are the Amott and USBM tests. They provide wettability indexes based on a combination of spontaneous and forced displacement properties of the oil/brine/rock system. They are very valuable for petrophysicists and reservoir engineers but take long to perform, up to several months, often even more than a year, and thus often come too late during reservoir pre-development evaluations.

In the last few years, there has been a growing interest in the assessment of wettability within the pore space, often associated with estimates of contact angles, interfacial curvature, or topological functions. These estimates have the advantage of considering millions of resolved pores. However, most of the calculated image-based wettability estimates often suffer from the lack of image resolution. Additionally, they might be influenced by the pore structure complexity.

In this paper, we explore the possibility of acquiring a qualitative wettability indicator, similar to that obtained using the conventional wettability characterization via Amott tests on centimeter-sized samples, using instead millimeter-sized samples imaged with a high-resolution micro-CT scanner. Following the idea presented in [6], also reported in [7] as a means of rapidly characterizing the wettability input required for Digital Rock Physics simulation, we used a similar experimental set-up to realize a full Amott-like cycle on small core samples (4mm diameter, 15mm long) with fluid saturations determined from micro-CT image analysis. It is also expected that pore scale imaging, at least in the part of pore network that can be fully resolved, will provide additional information on the wetting properties of the system. This approach was tested on two carbonate samples from the same reservoir. The duration of the proposed wettability assessment test may vary, in fact it depends strongly on the length of the ageing phase. In the presented examples, the wettability assessment was finished in nine weeks (wettability restauration, four weeks ageing and image analysis included).

2 Materials and methods

2.1 Rock samples and fluid properties

Two cylindrical samples of a reservoir carbonate rock were used in this study, their mineralogical composition is shown in Fig. 1.

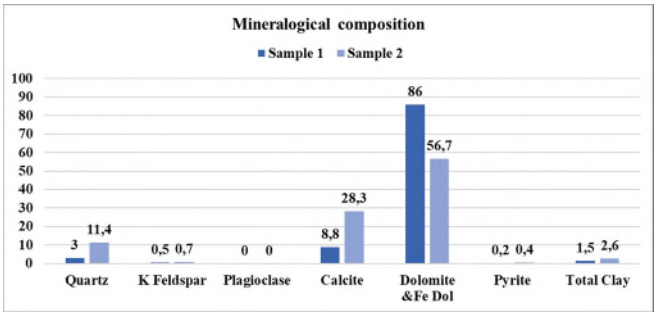

Fig. 1. Mini core samples mineralogical composition

* Corresponding author: repina.maria@totalenergies.com

Their main geometrical characteristics are provided in Table 1. Given the high degree of heterogeneity of the parent samples, the significant difference in the porosity values between the centimeter-sized and the milimeter-sized plugs is expected.

Table 1. Samples characteristics.

Sample	Length, mm	Diameter, mm	Porosity of the big parent plug, %	Permeability of the big parent plug, mD
1	13.95	3.91	20	20
2	14.50	3.90	8	16

The oil phase used was Marcol 52 (M52). The brine used for drainage and imbibition stages is a formation water dopped with KI, its composition is presented in Table 2.

Table 2. Brine composition.

Sel	C (g/L)
KI	100.0
NaCl	81.1
$CaCl_2$, 2H2O	14.5
$MgCl_2$, 6H2O	3.9
KCl	3.7
Na_2SO_4	1.5

For the characterization of the pore space with the Differential Imaging technique [3, 5], potassium iodide concentration was multiplied by three, following the example of [5] .

The dead oil used for the ageing comes from the field from which the carbonate reservoir samples were taken. This oil was centrifuged before being received; it was not filtered before the injection into the core.

2.2 Experimental program

The experimental program presented below, was applied to two samples.

Table 3 summarizes experimental temperature and pressure parameters.

Table 3. Experimental parameters.

Ageing temperature (°C)	95
Temperature during spontaneous and forced phases (°C)	28
Pore pressure during imaging (bar)	11
Confining pressure during imaging (bar)	50
Maximum confining pressure during forced phases (bar)	120
Maximum pore pressure during forced phases (bar)	100

2.2.1 Sample cleaning (carried out separately for both samples)

1. Sample was put in the Viton sleeve before being placed in a carbon flow cell
2. Confining pressure of 25 bars was applied and maintained within the cell to compress the Viton sleeve around the core sample to avoid fluid bypass. Temperature was raised to 65°C
3. 30 PV of 30 g/L NaCl/$CaCl_2$ (mass 90 %/10 %) brine was injected to wash out salts present in the sample
4. 95PV of toluene was injected at 5 µL/min
5. It was followed by the cyclic injection of toluene and mix of toluene and isopropanol in both directions. The cycles were composed of two phases: 30 PV at 5 µL/min toluene or toluene + isopropanol injection followed by maceration lasting between 2 and 8 hours. During the maceration period, the pore pressure was kept at 5 bars
6. Cleaning was finished with the injection of 78 PV of isopropanol at 10 µL/min
7. Sample was blown with the N_2
8. Temperature was lowered from 65°C to 28°C

2.2.2 Experimental protocol for porosity, saturation, and wettability characterization

For each sample, the experiment was performed as follows:

1. Core holder with the vertical flowing cell was installed into the micro-CT scanner
2. Four continuous tomograms “Dry scans” were taken for the whole sample with a voxel size 2.07 µm. The overlap of approximately 30% was used to stitch the four scans together
3. Vacuum was installed.
4. 25 PV of 300 g/L KI brine was injected into the rock sample to ensure that it was fully saturated with the highly contrasted brine. This step was necessary to characterize the sub-resolution pore space by applying the Differential Imaging method [3]. For more details, refer to the next section
5. Four continuous “KI_300” scans were taken for the whole sample with a voxel size 2.07 µm. Acquisition parameters were kept the same as for the dry scans.
6. High salinity brine was replaced by 48 PV of KI 100g/L brine. During the replacement brine injection, pressure was maintained close to 10 bars.
7. The primary drainage was effectuated by injecting 715 PV of the mineral oil M52 at 250µL/min. The direction was changed four times starting in a downwards direction. During the primary drainage, the confinement pressure was raised to 120 bars. SWi was fixed at 20-25%, with the most uniform SWi saturation profile. Fig. 2 shows the pressure recording during the primary drainage. The recovery pressure stayed equal at 11 bars.

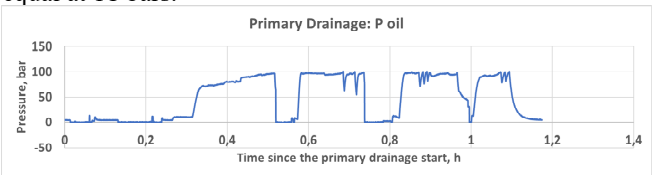

Fig. 2. Sample 1: Pressure monitoring during the primary drainage

8. Confinement pressure was decreased to 50 bars. The sample was moved to the oven.

9. 6 PV of toluene was injected to serve as a buffer between M52 and the dead oil.
10. M52 was replaced by the dead oil.
11. Four weeks ageing began. The temperature of the oven was kept at 95°C, pore pressure - at 6 bars. At the beginning of the second week, 6 PV of dead oil was injected at 0.6 µL/min in a downwards direction. One week after the direction of oil injection was changed, 700 µL of dead oil was injected at 0.6 µL/min. At the beginning of the last week of ageing, 6 PV of dead oil was injected at 0.6 µL/min one more time.
12. The temperature was progressively decreased to 65°C.
13. 6 PV of toluene was injected to serve as a buffer between dead oil and M52.
14. Dead oil was replaced by the mineral oil M52.
15. Four continuous "SWi_aged" scans were taken for the whole sample with a voxel size 2.07 µm. Acquisition parameters were kept the same as for the dry scans.
16. Flow cell was connected to the imbibition experimental set-up shown in Fig. 3.

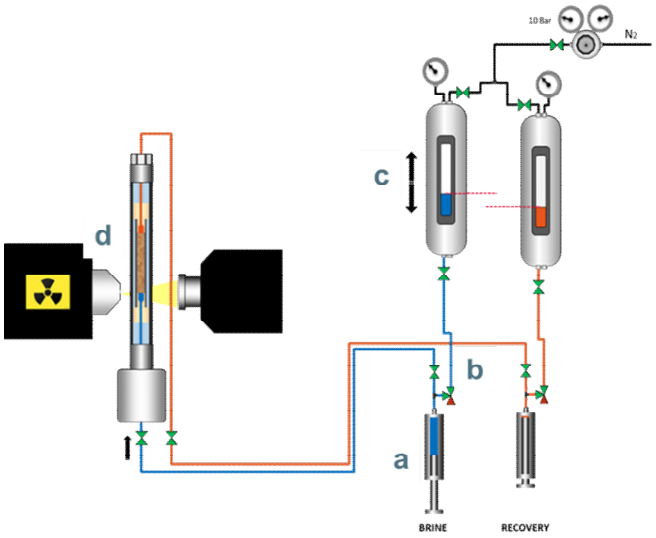

Fig. 3. Experimental set-up for the spontaneous imbibition: water level is controlled by the height of the water bottle. Steps indicated by a, b, b, d are detailed in the following paragraph.

17. The spontaneous imbibition was conducted as follows:
a) 5 PV of brine was injected at 0.6 µL/min to put the brine level at the inlet entrance, the brine arrival was controlled with the radio, as shown in Fig. 4

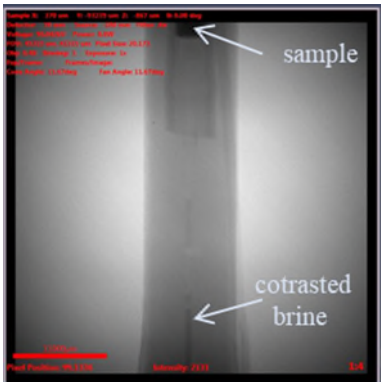

Fig. 4. Radio view: water rise in the tubing.

b) Injection was stopped, and the valve was switched. At that stage, the brine from the bottle started to interact with the sample and the recovery valve stayed opened.
c) Water bottle height was progressively adapted so that water pressure was sufficient to keep the brine level at the sample entrance, see Fig. 5.

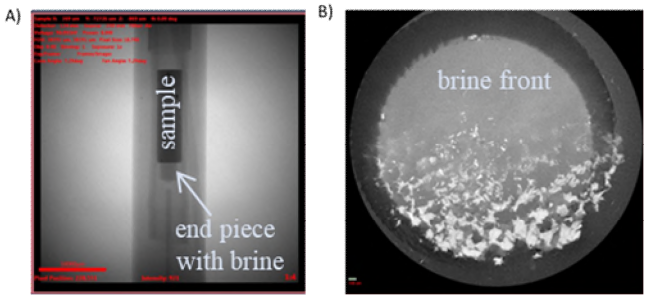

Fig. 5. Sample 1 A) Radio view: water in contact with the sample; B) image view: water in contact with the sample at the inlet

d) Over the next 6 days, the brine invasion was checked regularly with the radio and with the high-resolution acquisitions.
18. Four continuous "Spont_Imbib" scans were taken for the whole sample with a voxel size 2.07 µm. Acquisition parameters were kept the same as for the dry scans.

19. The line connected to the water bottle was closed. The forced imbibition began. It consisted of injecting:
a) 610 PV of the brine at the progressively increasing flow rate from 0.6 µL/min to 700 µL/min in the upward direction.
b) 350 PV of the brine at 700 µL/min in the downward direction.

The recovery and the confinement pressures were fixed at 11 and 120 bars respectively.

20. Confinement pressure was decreased to 50 bars. Brine pressure was regulated at 10 bars. The recovery valve was closed. Four continuous "Forced_Imbib" scans were taken for the whole sample with a voxel size 2.07 µm. Acquisition parameters were kept the same as for the dry scans.

21. The flow cell was connected to the drainage experimental set-up shown in Fig. 6

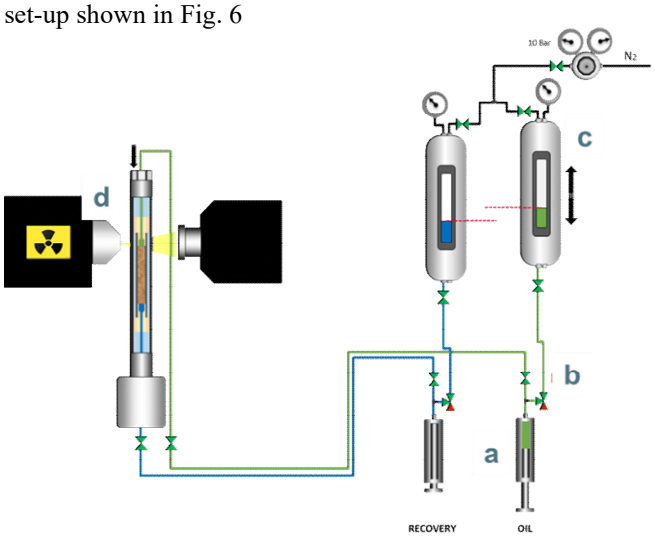

Fig. 6. Experimental set-up for the spontaneous drainage: M52 level is controlled by the height of the M52 bottle. Steps indicated by a, b, c, d are detailed in the following paragraph.

22. Spontaneous drainage was conducted as follows:
a) 15 PV of M52 was injected at 1 µL/min to fill the line connected to the sample and thus, put the M52 level at the inlet entrance. The arrival of the M52 was controlled with the X-ray monitoring in radio mode. Fig. 7 shows two stages: before and after M52 front arrival.

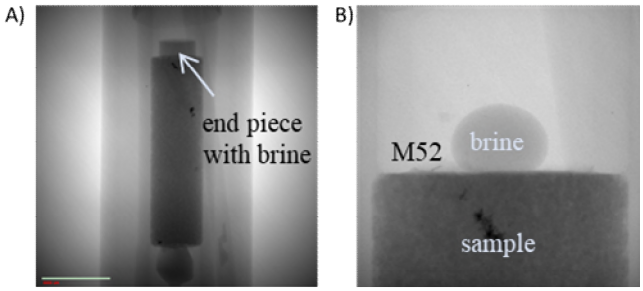

Fig. 7. A) Before: water in contact with the sample; B) After: zoom at the top of the sample: M52 pushed the water, however one water droplet stayed attached.

b) The injection was stopped, and the valve was switched. At that stage, M52 from the bottle started to interact with the sample and the recovery valve stayed opened.
c) Water bottle height was progressively adapted so that the M52 column pressure was sufficient to keep M52 level at the sample entrance.
d) Over the next 6 days, M52 spontaneous invasion was regularly checked in radio mode and with the high-resolution acquisitions.

23 Four continuous "Spont_Drain" scans were taken for the whole sample with a voxel size 2.07 µm. Acquisition parameters were kept the same as for the dry scans.

24. The line connected to the M52 bottle was closed. The forced drainage was started. It consisted of injecting:
a) 300 PV of M52 at the maximal possible flow rate in a downwards direction. The flow rate limitation was due to the max pressure limit equal to 100 bars. The max. constant injection flow rate that did not provoke the pump to shut down was equal to 60 µL/min
b) 300 PV at 60 µL/min in the upward direction
c) 325 PV at 55 µL/min in the downward direction.

The recovery and the confinement pressures were fixed at 10 and 120 bars respectively.

25. Confinement pressure was decreased to 50 bars. M52 pressure was regulated at 10 bars. The recovery valve was closed. Four continuous "Forced_Drain" scans were taken for the whole sample with a voxel size 2.07 µm. Acquisition parameters were kept the same as for the dry scans.

2.3 Imaging methods and processing

2.3.1 Imaging method

The images were taken by an Xradia Versa 520 high-resolution microCT. The X-ray energy was 90 kV and the power was 8W. The number of projections for each radio was 2001. The pixel size of all images was equal to 2.07 µm. All tomograms were reconstructed into 3D images using Zeiss reconstruction software.

Dry, KI_300, SWi_aged, Spont_Imbib., Forced_Imbib., Spont_Drain., Forced_Drain. images were first stitched together to cover the whole length of the sample. After, they were registered to the dry images to have the same orientation and to be easily comparable. A nonlocal means filter was used to remove noise. The image analysis was performed with the help of software packages: Mango [8] for the routine actions, ImageJ for the trainable Weka segmentation [2].

2.3.2 Characterization of the pore space and fluids inside

Differential imaging [3, 4] was used to quantify both resolvable and sub-resolution porosity. This method relies on the observation that the difference image between the KI saturated scan and the dry scan maximizes the phase contrast between grain, macro pores and zones containing sub-voxel porosity phases (Fig.8A – Fig.8C, zones 1-3 contain sub-resolution porosity) and consequently, provides a good input for image segmentation.

We clearly observe some sub-resolution pores with intermediate grey scale values in Fig. 8C. Results of the Weka trainable segmentation of the difference image can be found in Fig. 8D. Fig. 8E illustrates how good a trainable Weka segmentation is at capturing complex textures of the dual pore network.

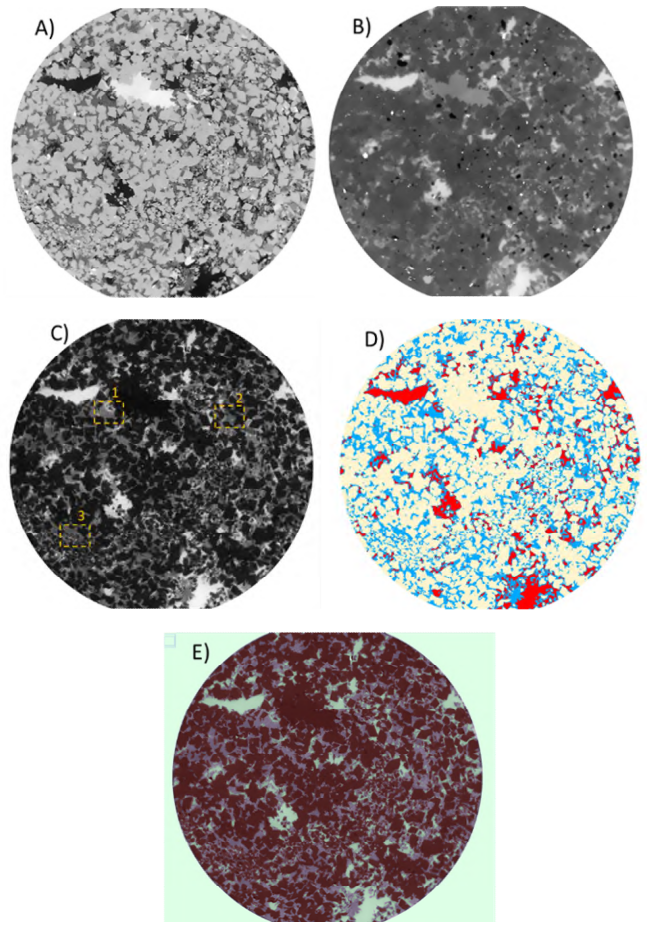

Fig. 8. Sample 2: two-dimensional cross-section of three-dimensional micro-CT images at the same location (13.18 mm from the sample inlet). A) dry scan; B) 300 g/L brine saturated scan; C) difference image between A and B; D) segmented difference image (resolved pores in red, unresolved porous zones in blue and tight grains in yellow); E) overlay of C and D images. Boxes 1-3 give examples of the zones containing sub-resolution porosity

Porosity of the sub-voxel zones was estimated based on the linear interpolation between two reference values (grey value of tight grains and grey value of brine in macro pores).

Fig.9 illustrates the profiles of total, macro and micro porosities for the second sample. As can be seen, the sample is heterogeneous in porosity. The mean total porosity slightly increases towards the outlet of the second examined mini core sample. As expected from the visualization of the pore network, a big part of the total porosity comes from the sub-voxel porosity.

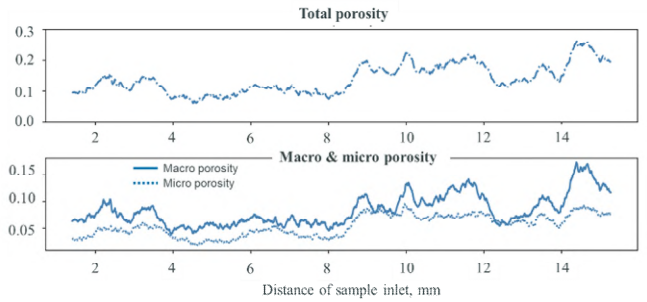

Fig. 9. Sample 2: porosity profiles along the sample length

Porosity quantification for samples 1 and 2 is given in Table 4.

Table 4. Porosity average values.

	Sample 1	Sample 2
Sub-resolution porosity	0.06 ± 0.01	0.06 ± 0.01
Resolved porosity	0.04	0.08
Total porosity	0.10 ± 0.01	0.14 ± 0.01

Two examples of the maps of the total (resolved and sub-voxel) porosity are illustrated in Fig.10.

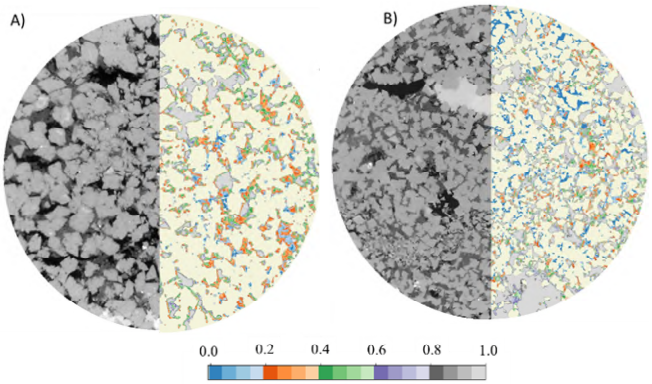

Fig. 10. Porosity map for A) Sample 1, slice is located at 12.68 mm from the inlet; B) Sample 2, slice is located at 13.18 mm from the inlet.

Grey-scale multiphase images for all stages of the second experiment are illustrated in Fig. 11 – Fig. 12. The black is mineral oil, the dark grey is grains, the light grey is doped brine.

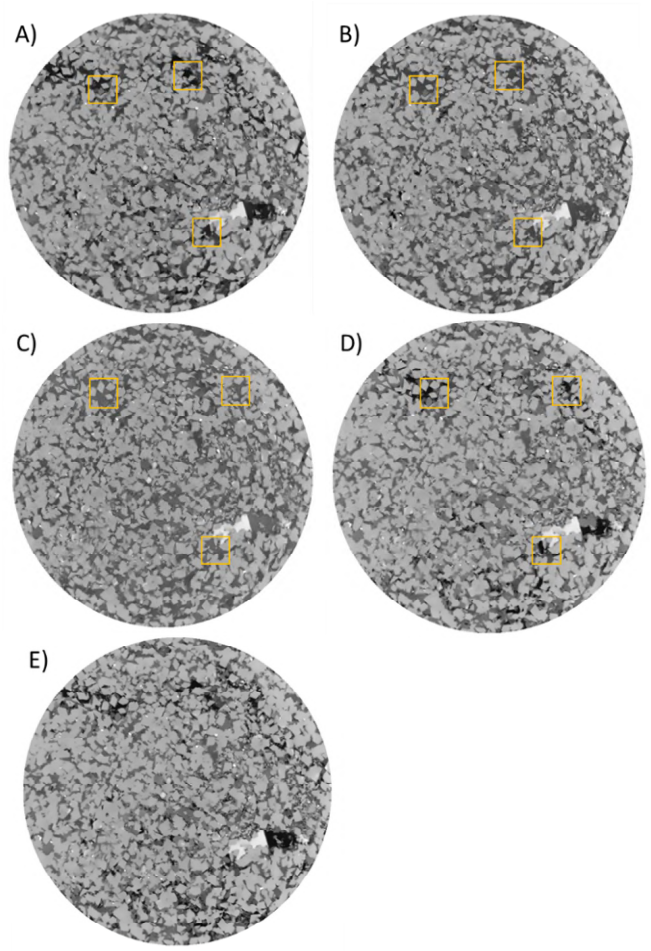

Fig. 11. Sample 1. Two-dimensional cross sections of three-dimentional micro-CT images. Slices are located at 1.56 mm from the bottom of the sample. Radius of each slice is equal to 1.53 mm. A) SWi_aged scan; B) Sp_Imbib scan; C) For_Imbib scan; D) Sp_drainage scan; E) For_Drainage scan. The yellow boxes indicate regions where fluid occupation was changed in comparison with the previous or the following saturation state

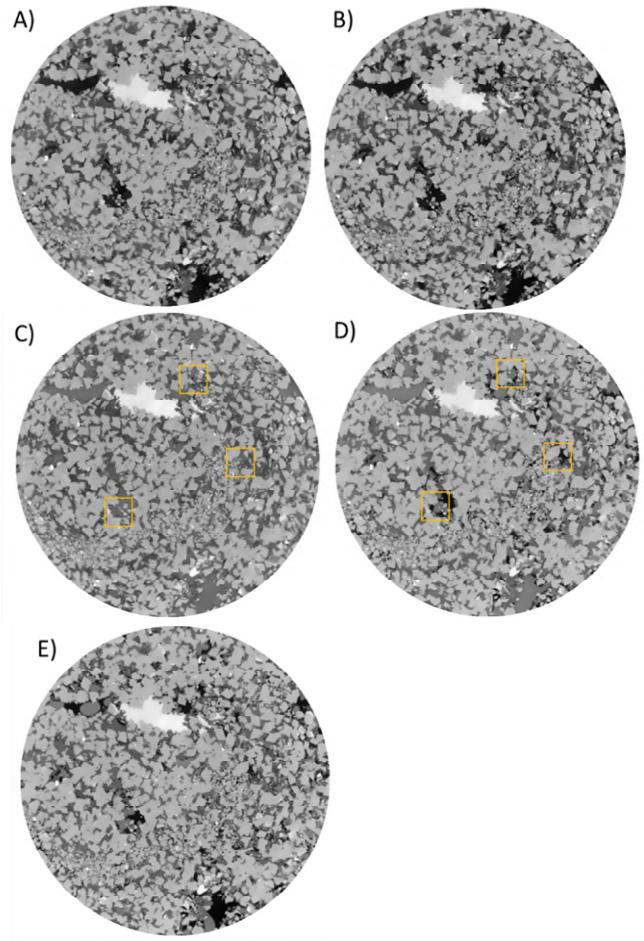

Fig. 12. Sample 2. Two-dimensional cross sections of three-dimensional micro-CT images. Slices are located at 13.18 mm from the bottom of the sample. Radius of each slice is equal to 1.53 mm. A) SWi_aged scan; B) Sp_Imbib scan; C) For_Imbib scan; D) Sp_drainage scan; E) For_Drainage scan. The yellow boxes indicate regions where fluid occupation was changed in comparison with the previous or the following saturation state

Fluid occupancy in the macro pores was identified by the direct two-phase segmentation using the converging active contour method with Mango software. Water saturation characterization in the sub-resolution pores was carried out following the principals of the differential imaging method.

The brine saturation profiles across the second sample are shown in Fig. 13.

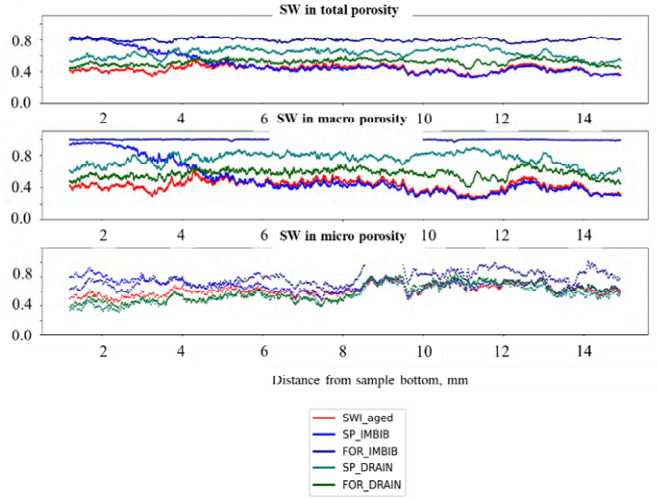

Fig. 13. Brine saturation profiles along the second sample from bottom to top: total; in macro pores; in sub-voxel zones. Brine access during the spontaneous imbibition was at the bottom, mineral oil access during the spontaneous drainage was at the top

It is apparent from Fig. 13 that the spontaneous imbibition of water happened only at the bottom, only one quarter of the sample had seen the increase of the water saturation coming principally from the macro pores. As for the spontaneous drainage, it was of higher intensity. Water saturation profiles suggest that it occurred along the entire sample, both macro and sub-resolution pores participated in the spontaneous drainage. Similar behaviour was seen for the first sample.

Average brine saturation values for both samples are presented in Table 5 – Table 6.

Table 5. Sample 1: water saturation average values.

	Ageing	Sp. Imb.	For. Imb.	Sp. Drn.	For. Drn.
Sub-resolution pores	0.60	0.48	1	0.86	0.80
Resolved pores	0.18	0.29	0.99	0.90	0.58
Total	0.46	0.48	0.99	0.87	0.72

Table 6. Sample 2: water saturation average values.

	Ageing	Sp. Imb.	For. Imb.	Sp. Drn.	For. Drn.
Sub-resolved pores	0.45	0.47	0.50	0.44	0.44
Resolved pores	0.42	0.50	0.99	0.75	0.57
Total	0.44	0.49	0.80	0.63	0.52

Table 5 and Table 6 illustrate that for both samples water saturation after the secondary drainage is higher than after the primary drainage. This increase of the water saturation was expected: during the secondary drainage it was much more difficult to inject M52 than during the first drainage. As a reminder, during the first and second drainage, the maximum accepted injection pressure was limited to 100 bars. During the second drainage, the maximum injection flow rate was divided by 4-5 vs. the primary drainage to respect the pressure limitation. This could suggest that during the four-week ageing, the initial wettability was shifted to a more oil-wet wettability, provoking more intensive water trapping that was noticed during the secondary drainage.

It should be noted that water saturation of the resolved porosity after the forced imbibition might be overestimated. In fact, the volume of oil films on the rock surface cannot be quantified with a high degree of precision, because it is below image resolution. The uncertainty of the saturation after this step is the highest, it is estimated at 3-5 %.

2.4 Wettability analysis results and discussions

To characterize the wettability behavior, we proposed to conduct the Amott–like test on two mini-core samples. This test includes a four-displacement sequence, similar to that of an Amott test, starting from the irreducible saturation state after ageing. It assumes that each sample is subjected to spontaneous and forced flows, first by water (imbibition) and afterwards by oil (drainage). The spontaneous flows are capillary driven. The forced flows are implemented by viscous displacement.

A pseudo-wettability index is proposed to be calculated by the following Eq. 1:

$$I_w - I_o = \frac{S_w^{sp.imb} - S_w^{Swi}}{S_w^{for.imb} - S_w^{Swi}} - \frac{S_o^{sp.dr} - S_o^{for.imb}}{1 - S_w^{for.dr} - S_o^{for.imb}} \quad (1)$$

Where I_w – is imbibition index, I_o – is drainage index, sp.imb and sp.dr are spontaneous imbibition and drainage, for.imb and for.dr are forced imbibition and drainage. This index is comprised between +1 and -1, it refers to the quantitative degree of wettability like the Amott-Harvey index [1].

Table 7 shows the results of pseudo-wettability index calculation for two samples.

Table 7. Result of pseudo-wettability index calculation.

	Sample 1			Sample 2		
	Iw	Io	Iw- Io	Iw	Io	Iw- Io
All pores	0.04	0.44	-0.41	0.14	0.61	-0.47

Results obtained from the pseudo-wettability index calculation suggest that the studied rock-fluids systems are most probably oil wet, for both samples the drainage index is systematically much higher than the imbibition index.

Moreover, this conclusion is supported by the following experimental observations:

1) Difficulty in setting Swi: for both samples, total initial water saturation remains high, suggesting capillary trapping of water

2) For both samples, the spontaneous imbibition remains limited to the lower part of the sample. The increase of water saturation after the spontaneous imbibition might be even attributed to the initial water advancement provoked under the initial non-stabilized pressure of the water bottle. For this reason, it was advised to adapt the experimental set-up to rule out, or at least substantially reduce the probability of the accidental forced imbibition at the sample inlet

3) Spontaneous drainage, on the other hand, happened over the entire length of the sample. We found a clear oil saturation increase in both resolved and the sub-resolution porosity across two samples. Moreover, we even recorded in the radio

mode M52 production at the bottom of the second sample during the first 6 days, as shown in Fig. 14

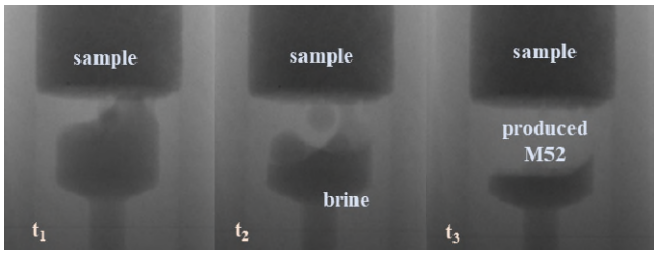

Fig. 14. Bottom of the second sample imaged in the radio mode during the spontaneous drainage: M52 production over time

4) Distribution of oil and brine visible interfaces within the resolved pores also suggests oil wettability, Fig. 15

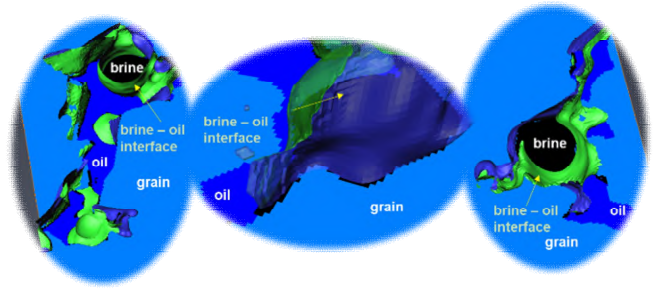

Fig. 15. Examples of some resolved pores of the first sample with brine-oil interfaces having negative curvature and occupying the large pore spaces

3 Conclusions

To assess the wettability of reservoir samples in a quick and physically meaningful manner, we designed a new experimental set-up allowing us to carry out a full Amott-like cycle on a small core sample imaged with a high-resolution micro-CT scanner.

The advantage of this kind of experiment is that it provides global wettability characterization based on multiple experimental observations, the analysis of the fluid distribution in the porous space and the result of the pseudo-wettability index calculation. Moreover, it respects the experimental sequence of the industry standard Amott test, yet with a significantly reduced test duration. Thanks to the high-quality 3D imaging, it provides complementary information describing the spatial distribution of the fluids in the visible pore network during spontaneous and forced phases. On top of that, it is less sensitive to imaging resolution than existing approaches based on topological characteristics and contact angles.

Comparison with the results of conventional Amott test on neighbour centimeter-sized core samples was planned and initiated in parallel to the Amott-like image-based tests on small core samples. These standard tests are still in progress. Future work should involve the comparison of the results of the wettability characterization on small core samples with the proposed experimental design to the results of the standard Amott ones.

References

[1] Amott, E. 1959. Observations Relating to the Wettability of Porous Rock. *Trans.* 216, 01, 156–162.

[2] Arganda-Carreras, I., Kaynig, V., Rueden, C., Eliceiri, K. W., Schindelin, J., Cardona, A., and Sebastian Seung, H. 2017. Trainable Weka Segmentation: a machine learning tool for microscopy pixel classification. *Bioinformatics (Oxford, England)* 33, 15, 2424–2426.

[3] Gao, Y., Lin, Q., Bijeljic, B., and Blunt, M. J. 2017. X-ray Microtomography of Intermittency in Multiphase Flow at Steady State Using a Differential Imaging Method. *Water resources research* 53, 12, 10274–10292.

[4] Gao, Y., Raeini, A. Q., Selem, A. M., Bondino, I., Blunt, M. J., and Bijeljic, B. 2020. Pore-scale imaging with measurement of relative permeability and capillary pressure on the same reservoir sandstone sample under water-wet and mixed-wet conditions. *Advances in Water Resources* 146, 2, 103786.

[5] Lin, Q., Al-Khulaifi, Y., Blunt, M. J., and Bijeljic, B. 2016. Quantification of sub-resolution porosity in carbonate rocks by applying high-salinity contrast brine using X-ray microtomography differential imaging. *Advances in Water Resources* 96, 306–322.

[6] Regaieg M, Brugidou R and Nono, F. 2022. *A porous sample wettability parameter determining method and related system,* US Patent No. 63/342,923.

[7] Regaieg M, Nono F, Farhana Faisal T, Varloteaux C and Rivenq R. 2022. Pore network simulations coupled with innovative wettability anchoring experiment to predict relative permeability of a mixed-wet rock. *Symposium of the Society of Core Analysis* (2022).

[8] Sheppard, A. *MANGO*. ANU.